

Article

Incorporating Cerium Vanadate into Multi-Walled Carbon Nanotubes for Fabrication of Sensitive Electrochemical Sensors toward Sulfamethazine Determination in Water Samples

Jingying Ma ¹, Chaoyan Zhang ², Xiaoping Hong ^{2,*} and Jiyang Liu ^{2,*} ¹ Department of Construction, Zhejiang College of Construction, Hangzhou 311231, China² Department of Chemistry, Key Laboratory of Surface & Interface Science of Polymer Materials of Zhejiang Province, Zhejiang Sci-Tech University, Hangzhou 310018, China

* Correspondence: xpnhong@zstu.edu.cn (X.H.); liujy@zstu.edu.cn (J.L.)

Abstract: We developed a simple hydrothermal technique for the fabrication of a flexible integrated composite containing cerium vanadate (CeVO₄) and multi-walled carbon nanotubes (MWCNTs). The CeVO₄/MWCNTs composite possessed good conductivity and interesting electrochemical catalytic performance when immobilized on a glassy carbon electrode (GCE). This CeVO₄/MWCNTs-GCE sensor provided excellent analytical performance for the detection of the sulfonamide antibacterial drug sulfamethazine (SMZ). Benefiting from the significantly enlarged surface area of the modified electrode and the catalytic effect of CeVO₄-MWCNTs, the sensor offered high sensitivity, good stability, fine selectivity, and a remarkable limit of detection (LOD) of 0.02 μM. Furthermore, the sensor also exhibited ideal performance with good recovery and precision when applied to SMZ residue detection in real aquaculture water samples.

Keywords: carbon nanotubes; cerium vanadate; sensors; sulfamethazine



Citation: Ma, J.; Zhang, C.; Hong, X.; Liu, J. Incorporating Cerium Vanadate into Multi-Walled Carbon Nanotubes for Fabrication of Sensitive Electrochemical Sensors toward Sulfamethazine Determination in Water Samples. *Chemosensors* **2023**, *11*, 64. <https://doi.org/10.3390/chemosensors11010064>

Academic Editors: Maria Luz Rodriguez-Mendez and Alain Walcarius

Received: 23 November 2022

Revised: 7 January 2023

Accepted: 12 January 2023

Published: 13 January 2023



Copyright: © 2023 by the authors. Licensee MDPI, Basel, Switzerland. This article is an open access article distributed under the terms and conditions of the Creative Commons Attribution (CC BY) license (<https://creativecommons.org/licenses/by/4.0/>).

1. Introduction

Sulfonamides such as sulfadiazine (SD), sulfamethazine (SMZ), sulfamethoxazole (SMX), and sulfamethoxine (SMOX) are a class of antibacterial drugs that possess structures similar to that of p-aminobenzenesulfonamide. As a class of broad-spectrum antibacterial agents, sulfonamides were widely used to treat bacterial infections in humans during the early 20th century. Recently, owing to their abundance, low cost, and safety, sulfonamides are more commonly used for treating animals. Typically, sulfonamides are usually used as animal feed additives for prophylactic and therapeutic purposes. However, the overuse or improper use of these veterinary drugs leads to the presence of excessive drug residues in animal-origin products as well as the potential risk of environmental pollution [1]. Although the residues of sulfonamides are usually very low in the environmental background, their concentration may be found increasing significantly in the wastewater [2]. In the aquaculture industry, fish food containing sulfonamide additives is commonly thrown into aquaculture waters to feed the fish. Most of these drug additives are therefore released into water systems, forming a new type of pollution that is a critical threat to public health. An increasing amount of clinical evidence has indicated that sustained exposure to sulfonamides in food or the environment has a potentially negative impact on health. This includes increased bacterial resistance, liver and renal injury, carcinogenic effects, and mutagenic action. Accordingly, strict laws or principles have been developed by governments and other organizations to regulate the content of sulfonamide residues in food or the environment. Therefore, simple, sensitive, and selective techniques are needed for the determination of trace concentrations of sulfonamide residues. Common techniques such as high-performance liquid chromatography (HPLC) [3], mass spectrometry [4], fluorescence spectroscopy [5], and enzyme-linked immunosorbent assay (ELISA) [6] have

been successfully applied for the accurate determination of sulfonamide residues in terms of good resolution, excellent repeatability and precision, linear output, and satisfactory reliability. However, the main disadvantage of these traditional detection methods is the requirement of expensive devices with sophisticated operations, time-consuming procedures, and offline-only application. This has limited the application of these techniques for controlling antibacterial drug pollution in food or environmental backgrounds.

Electrochemical techniques offer remarkable advantages over classical methods in terms of analytical speed, low cost, equipment miniaturization, and in situ measurement or automatic application [7–9]. Scientists in this field have proposed various electrochemical devices for the convenient analysis of antibacterial drug residues [10,11]. In particular, chemically modified electrodes (CMEs) can be fabricated by electrode surface modification. These electrodes exhibit excellent performance due to their faster electron transfer kinetics, catalytic effect, and larger active surface area, resulting in improved sensitivity and selectivity as well as a lower detection limit [12–14]. Carbon nanomaterials, such as graphene [15–17], carbon quantum dots [18–22], carbon nanotubes [23], and their composite materials [24–26], have been successfully applied as functional blocks (e.g., probes, enhanced materials, carriers) for fabricating various sensors and have achieved improved analytical performance. Carbon nanotubes (CNTs) are a typical class of nanomaterial that possess excellent conductivity, high specific surface area, a superior electrocatalytic effect, and good antifouling performance [27]. Therefore, CNTs are an ideal material for CME preparation. A variety of electrochemical sensors based on CNTs have been invented to analyze organic or inorganic substances.

Metal oxides, especially nanostructured rare earth metal oxides, have been successfully used for preparing CMEs. Owing to their remarkable physicochemical properties, such as their nanoscale effect, mixed valence states, tunable bandgaps, and abundant oxygen vacancies, CMEs based on nanostructured rare earth metal oxides can show enhanced electrochemical behavior [28]. Đurović and coworkers developed a ZnO/reduced graphene modified electrode that exhibited a remarkable performance for the determination of tetracycline determination [29]. A samarium vanadate nanoparticle-based sensor was successfully fabricated for sulfadiazine analysis, demonstrating excellent sensitivity and selectivity [30]. In Kokulnathan's work, hedgehog-like cerium vanadate particles were successfully interconnected with carbon nanofibers to form an electrochemical sensor for the sensitive detection of the drug nilutamide [28]. Sharma and coworkers reported a screen-printed electrode based on flower-like cerium vanadate and graphitic carbon nitride for sensitive and real-time monitoring of mesalazine [31]. Metal oxides exhibit poor conductivity when they are used as electrode materials by themselves [32]. Therefore, the incorporation of metal oxides into conductive nanomaterials with high specific surface areas to form new composites has great potential for the fabrication of CMEs with better analytical performance.

In this work, a new functional electrochemical CME was prepared by fabricating a composite material integrating multi-walled carbon nanotubes (MWCNTs) and cerium vanadate particles (CeVO_4). Herein, this CeVO_4 /MWCNTs composite was synthesized by the hydrothermal method and employed for the fabrication of new electrochemical sensors. The encouraging analytical performance of these sensors was demonstrated through the electrochemical determination of SMZ in aquaculture water samples with or without residues. The developed electrochemical sensor has advantages of simple fabrication, easy operation, and high sensitivity owing to the good conductivity, enlarged surface area, and high electrochemical catalytic of CeVO_4 -MWCNTs nanocomposites.

2. Materials and Methods

2.1. Materials

High-purity multi-walled carbon nanotubes (MWCNTs) were purchased from Jichang Nano Co., Ltd. (Nanjing, China). Analytical grade cerium chloride ($\text{CeCl}_3 \cdot 7\text{H}_2\text{O}$), ammonium metavanadate (NH_4VO_3), and SMZ were supplied by Sigma Aldrich (Shanghai,

China). Sodium dodecyl sulfonate (SDS) and other analytical grade chemicals were obtained from Chinses Chemical (Shanghai, China). Ultrapure deionized water was prepared by an Academic Millipore system (Millipore Inc., Billerica, MA, USA) for use in all experiments.

2.2. Apparatus

A CHI660E electrochemical station (Chenhua, Shanghai, China) equipped with a three-electrode system (a saturated AgCl/Ag reference electrode, a Pt wire counter electrode, and a prepared CME as the working electrode) was applied for electrochemical testing. The morphologies and elemental information of the composite were investigated by a field-emission-scanning electron microscope (FE-SEM, ZEISS Sigma 300) equipped with a Smart EDX energy-dispersive X-ray spectrometer (EDS). X-ray diffraction (XRD, Rigaku Smart Lab 9kW, Tokyo, Japan) was used to analyze the phases of the composite. The structure of the composite was further investigated by a Raman spectrometer (Horiba Scientific-Lab RAM HR Evolution, Kyoto, Japan). X-ray photoelectron spectroscopy (XPS) was performed using a Thermo Scientific instrument (Thermo Scientific K-Alpha, Boston, MA, USA).

2.3. Preparation of CeVO₄/MWCNTs Composite

The preparation of the CeVO₄/MWCNTs composite followed a slightly modified literature method [33]. Briefly, 0.02 M cerium chloride and 0.02 M SDS were dissolved in 50 mL deionized water to form a yellow-colored solution. An appropriate amount of MWCNT powder was added to this solution, which was stirred to ensure good mixing. After gradually adding 50 mL of 0.02 M NH₄VO₃ into the solution, the reaction system was ultrasonicated for 30 min. Next, the resulting black solution was transferred into a Teflon-lined stainless-steel autoclave and heated at 180 °C for 12 h. After the hydrothermal reaction, the autoclave was cooled to room temperature. Then, the precipitate was separated by filtration, rinsed several times with deionized water, and dried in a vacuum oven at 60 °C for 24 h. This composite product was denoted CeVO₄/MWCNTs.

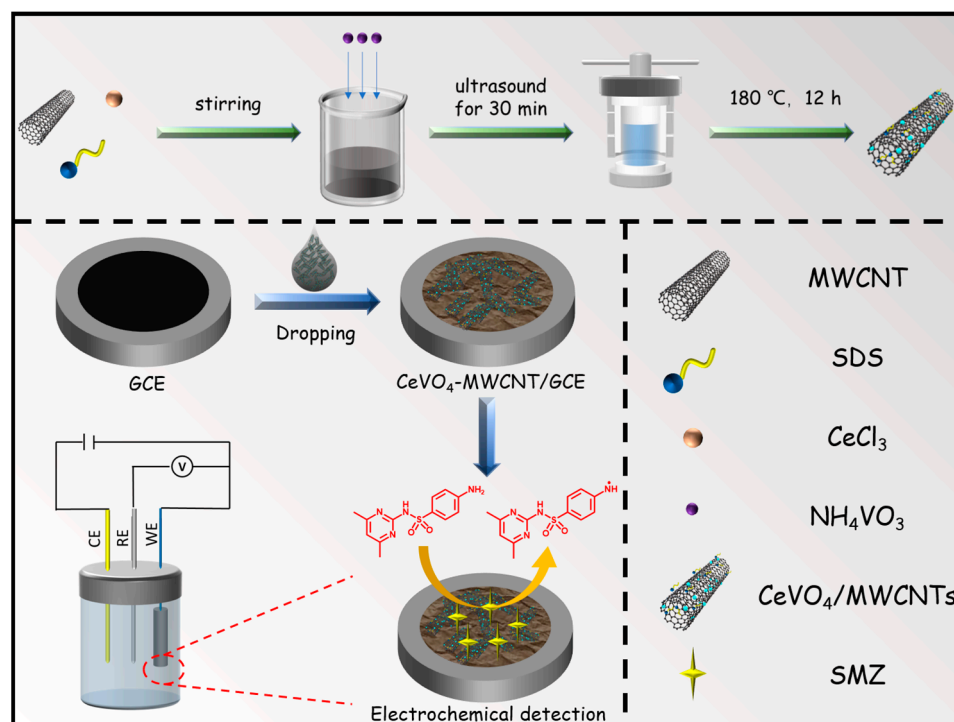
2.4. Fabrication of CeVO₄/MWCNTs-GCE

The prepared CeVO₄/MWCNTs was finely ground in an agate mortar. 5.0 mg of the ground CeVO₄/MWCNTs black powder was then transferred into 5.0 mL deionized water, which was vigorously stirred for 10 min by an ultrasonic agitator to form a uniform black gel. A proper volume of this black gel was cast onto a finely polished GCE-based electrode substrate. The solvent was allowed to evaporate in a clean ambient atmosphere to form a new CME, denoted CeVO₄/MWCNTs-GCE. For comparison, CMEs denoted MWCNTs-GCE and CeVO₄-GCE were prepared by a similar procedure.

3. Results and Discussion

3.1. Convenient Fabrication of CeVO₄/MWCNTs-GCE

Scheme 1 illustrates the synthesis strategy for preparing CeVO₄/MWCNTs-GCE. First, the CeVO₄/MWCNTs composite was synthesized using cerium chloride hydrate, ammonium metavanadate, SDS, and MWCNTs via a hydrothermal route followed by separation. After drying in a vacuum oven at 60 °C for 24 h, the obtained black filter cake was thoroughly ground in an agate mortar. Then, 5 mg black powder was dispersed into deionized water to form a uniform gel with the help of ultrasonic agitation. Finally, a drop of this black gel was carefully cast onto the surface of a finely polished GCE, followed by mild evaporation of the solvent in the ambient atmosphere. A CME denoted CeVO₄/MWCNTs-GCE was obtained for subsequent analytical experiments. For comparison, MWCNTs-GCE and CeVO₄-GCE were prepared in parallel following similar pathways.



Scheme 1. The preparation and application of CeVO₄-MWCNTs.

3.2. Raman Spectroscopy and Morphological Analysis

Raman spectroscopy and SEM were used to verify the synthesis of the CeVO₄-MWCNTs composite. The Raman spectrum of MWCNTs (Figure 1a) featured a typical disordered band (D band) at 1340 cm⁻¹, which was ascribed to single-bonded sp³ hybridized carbon. The graphitic band (G band) at 1578 cm⁻¹ was assigned to sp² hybridized carbon. A conspicuous broad band, known as the 2D band, was also observed at 2684 cm⁻¹ [34]. In the CeVO₄/MWCNTs spectrum, the D, G, and 2D bands appeared at 1346, 1586, and 2689 cm⁻¹, respectively, slightly shifting toward higher wavenumbers. This was indicative of the increased dispersibility of the MWCNTs after chemical modification [35]. Furthermore, the ratio of D band and G band intensities (I_D/I_G) decreased from 1.17 to 0.95 after modification. This implied that the sp³ hybridized carbon (such as the amorphous carbon introduced during the preparation of the MWCNTs) was removed during the fabrication of the CeVO₄/MWCNTs composite [36]. Bands at 794 cm⁻¹ and 861 cm⁻¹ were attributed to the symmetric and antisymmetric stretching of VO₄³⁻, which was in good agreement with other literature [37].

The morphology and elemental composition of the composite were characterized by a ZEISS Sigma 300 FE-SEM coupled with EDS. As shown in Figure 1c, the MWCNTs fibers were clear and distinct, and they did not show the presence of any contaminants. However, needle-like particles scattered across the MWCNTs fibers were observed in the SEM image of CeVO₄/MWCNTs (Figure 1d). EDS analysis of CeVO₄/MWCNTs (Figure 1e) demonstrated the presence of C, O, Ce, and V elements, with atomic percentages of 73.72%, 19.70%, 2.73%, and 2.30%, respectively. The Ce/V atomic ratio was approximately equal to 1, consistent with the proportion of cerium and vanadium in CeVO₄ molecules. EDS mapping shows that C, O, Ce, and V were homogeneously dispersed throughout the CeVO₄/MWCNTs composite sample (Figure 1f–i).

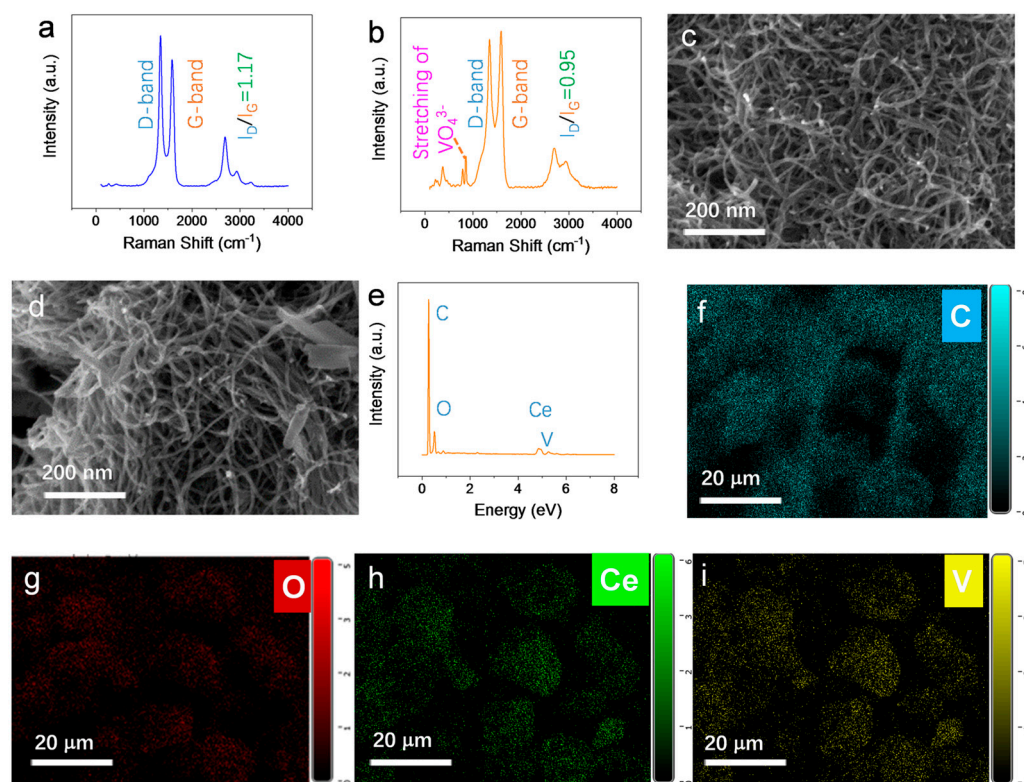


Figure 1. Raman spectra of (a) MWCNTs and (b) $\text{CeVO}_4/\text{MWCNTs}$. SEM images of (c) MWCNTs and (d) $\text{CeVO}_4/\text{MWCNTs}$. (e) EDS spectrum of $\text{CeVO}_4/\text{MWCNTs}$. (f–i) EDX mapping of $\text{CeVO}_4/\text{MWCNTs}$ showing the distribution of C, O, Ce, and V.

3.3. Lattice and Valence Analysis of $\text{CeVO}_4/\text{MWCNTs}$

XRD patterns of CeVO_4 , MWCNTs, and $\text{CeVO}_4/\text{MWCNTs}$ were obtained to evaluate their crystal structures, as illustrated in Figure 2a. The CeVO_4 sample showed well-defined and high-intensity diffraction peaks corresponding to the structure of tetragonal CeVO_4 (JCPDS no. 12-0757). The MWCNTs diffraction peaks at $2\theta = 25.9^\circ$ and 43.4° corresponded with those from literature reports [38]. Impressively, the typical intense diffraction peaks of CeVO_4 and weak, but well-defined, MWCNTs peaks were observed in the XRD pattern of the $\text{CeVO}_4/\text{MWCNTs}$ composite, implying the successful preparation of this composite. The composition and elemental valence states of the $\text{CeVO}_4/\text{MWCNTs}$ composite were analyzed by XPS. The survey spectrum in Figure 2b showed an intense peak at about 286.4 eV, which was ascribed to the C 1s binding energy. O 1s, V 2p, and Ce 3d peaks were, respectively, observed at about 533.3, 516.3, and 885 eV. The high-resolution and deconvoluted C 1s, O 1s, Ce 3d, and V 2p XPS spectra of $\text{CeVO}_4/\text{MWCNTs}$ are shown in Figure 2c–f. As shown in Figure 2c, C 1s peak was fitted with four deconvoluted peaks at 284.5, 285.1, 286.6, and 290.4 eV, which corresponded to the binding energies of sp^2 carbon (C=C), sp^3 carbon (C-C), C-O, and the $\pi\text{-}\pi^*$ shake-up feature, respectively. This was consistent with the carbon valence information of MWCNTs pretreated by strong acid for the promotion of hydrophilicity [39]. The deconvoluted O 1s spectrum (Figure 2d) displayed an obvious peak at 529.5 eV corresponding to the oxide bonds of lattice oxygen in tetragonal CeVO_4 [40], a moderate peak at 531.3 eV related to the oxygen of OH^- ions adsorbed on the CeVO_4 lattice [33], and a weak peak at 532.9 eV associating with the oxygen in C-O bonds or water molecules adsorbed on the sample surface [36]. As shown in Figure 2e, two pairs of obvious Ce 3d peaks were observed at 903.3, 899.3 eV and 884.9, 881.2 eV. These pairs of peaks were ascribed to the binding energies of Ce 3d_{3/2} and Ce 3d_{5/2}, respectively, in agreement with Yang's report [40]. The V 2p spectrum of $\text{CeVO}_4/\text{MWCNTs}$ shown in Figure 2f showed two strong peaks at 516.7 and 523.9 eV,

which represented the V 2p_{3/2} and V 2p_{1/2} binding energies attributed to the pentavalent state of vanadium (V⁵⁺) [31].

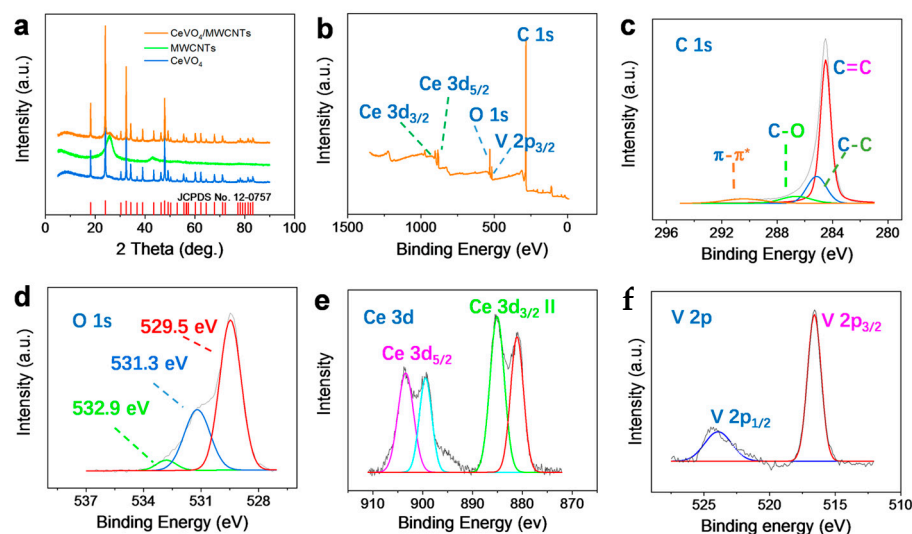


Figure 2. Structural characterization. (a) XRD patterns of CeVO₄, MWCNTs, and CeVO₄/MWCNTs. (b) XPS survey spectrum of CeVO₄/MWCNTs. (c–f) Deconvoluted C 1s, O 1s, Ce 3d, and V 2p XPS spectra of CeVO₄/MWCNTs.

3.4. Electrochemical Analysis

EIS was used to investigate the electrochemical properties of the prepared electrodes. Nyquist plots were obtained for bare GCE, CeVO₄-GCE, MWCNTs-GCE, and CeVO₄/MWCNTs-GCE in 0.1 M of KCl containing 5 mM K₃[Fe(CN)₆]/K₄[Fe(CN)₆], as shown in Figure 3a. In these plots, the semicircles related to the charge-transfer resistance (R_{ct}) were observed at a high-middle frequency range. Larger semicircles indicate a higher R_{ct} , resulting in lower electrode conductivity [41,42]. GCE had the second-largest semicircle, implying a moderate charge-transfer resistance. After CeVO₄ modification, CeVO₄-GCE possessed the largest semicircle (R_{ct}) due to the poor conductivity of CeVO₄. However, owing to the good conductivity of MWCNTs, the MWCNTs-GCE electrode exhibited a significantly smaller semicircle, indicating a significant decline in R_{ct} and much higher conductivity. As expected, when CeVO₄/MWCNTs was used as the modifier, the R_{ct} of the as-prepared electrode slightly increased but was still lower than that of GCE. This demonstrated the successful preparation of CeVO₄/MWCNTs-GCE. However, in Figure 3a, small arcs can also be found in the high frequency region on the left side of the high-middle frequency semicircle, which indicates that there are two complex interfacial transfer processes on the modified electrode surface. This phenomenon probably attributed to the fact that CeVO₄/MWCNTs and other modifiers did not completely cover the surface of the glassy carbon electrode during the preparation of the modified electrode, resulting in part of the exposed surface of the GC electrodes and the modified layers being involved in the interfacial transfer of electrons at the same time [43,44].

Cyclic voltammetry (CV) was employed to evaluate the electrochemical performance of the modified electrodes in 0.1 M sulfuric acid solution containing 0.1 mM SMZ with a potential scan rate of 50 mV/s. CeVO₄/MWCNTs-GCE, CeVO₄-GCE, MWCNTs-GCE, or bare GCE were applied as the working electrode, a clean platinum wire was used as the counter electrode, and AgCl/Ag (saturated KCl) was the reference electrode. As shown in Figure 3b, a tiny anodic current peak was observed at 1.02 V and no corresponding cathodic peak appeared during the reverse scanning process. This corresponded to a possible oxidation due to the reaction of one proton and one electron of the primary amino group of SMZ, leading to the subsequent formation of a dimer [45]. Compared with bare GCE, no significant change in the anodic peak was observed at a similar potential when CeVO₄-GCE

was used as the working electrode. Notably, an obvious and negatively shifted anodic peak at 0.95 V was observed when MWCNTs-GCE was used as the working electrode, which was in good agreement with our previous work [46]. The significant increase in the current response was attributed to the large specific surface area of the MWCNTs and their good conductivity. Based on the structure of SMZ and MWCNTs, π - π interaction, hydrophobic interaction, hydrogen bonding effects were also possible mechanisms for promotion of the detection of SMZ [47]. Excitedly, the anodic peak of SMZ was dramatically amplified when the CeVO₄/MWCNTs-GCE electrode was used. This phenomenon was due to the synergistic performance of CeVO₄ and MWCNTs. Namely, the MWCNTs provided a large electrochemical active surface and good conductivity, while CeVO₄ owned potent electrocatalytic performance, leading to an increase in the electron transfer between the analyte and the electrode surface. Furthermore, the anodic potential of SMZ was negatively shifted to 0.85 V, suggesting a convenient reduction in anodic interference during the amperometric analysis. Therefore, CeVO₄/MWCNTs-GCE is suitable for the electrochemical analysis of SMZ.

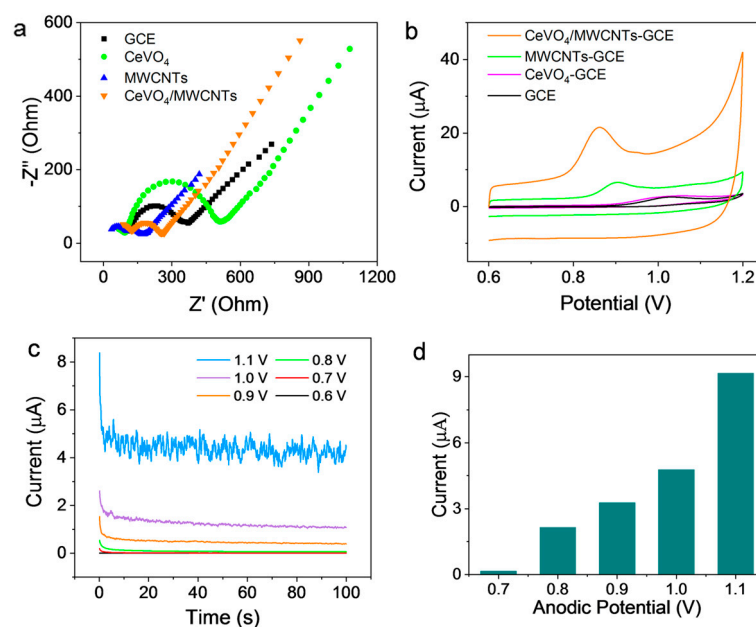


Figure 3. Electrochemical characterization. (a) Nyquist plots of different working electrodes (bare and coated GCE) obtained in 0.1 M KCl containing 5 mM K₃[Fe(CN)₆]/K₄[Fe(CN)₆], (b) CV response of the working electrodes obtained in 0.1 M sulfuric acid containing 0.1 mM of SMZ, (c) amperometric response of CeVO₄/MWCNTs-GCE obtained at different anodic potentials in 0.1 mM SMZ solution, and (d) dependence of response current on anodic potential.

Amperometry is an excellent quantitative method due to its ultra-high sensitivity and ease of online analysis or automated analysis [48–50]. The working potential was optimized by applying significant anodic potentials of 0.6, 0.7, 0.8, 0.9, 1.0, and 1.1 V in 0.1 M sulfuric acid containing 0.1 mM SMZ. The anodic currents obtained with CeVO₄/MWCNTs-GCE slightly increased when the anodic potential was raised from 0.6 V to 0.8 V, but significantly increased when the anodic potential was raised from 0.9 V to 1.1 V (Figure 3c,d). The anodic current obtained at 1.1 V was significantly higher than that obtained at 1.0 V and 0.9 V, but the current noise was also extremely high (Figure 3c), implying negligible background interference during the analysis procedure. To avoid excessive current noise and to obtain a sensitive anodic current response, 0.9 V was set as the optimal anodic potential for the amperometric analysis of SMZ in subsequent experiments.

3.5. Analytical Performance of $\text{CeVO}_4/\text{MWCNTs-GCE}$ toward SMZ

Under optimal conditions, the performance of $\text{CeVO}_4/\text{MWCNTs-GCE}$ toward the quantitative detection of SMZ was investigated by amperometric technique. According to the optimized parameters, the working anodic potential was 0.9 V, and a series of strictly metered volumes of SMZ stock solution was successively spiked into an electrochemical cell containing 5.0 mL of 0.1 M sulfuric acid with the aid of constant stirring. As shown in Figure 4a, the anodic current rapidly rose after each spiking of SMZ stock solution and then leveled off after 10 s. Therefore, the response time of the sensor was estimated to be 10 s. Furthermore, the increase in anodic current was dependent on the concentration of SMZ in the electrochemical cell. The $\text{CeVO}_4/\text{MWCNTs-GCE}$ electrode displayed different linear correlations when exposed to low or high concentrations of SMZ. A linear correlation equation of $I (\mu\text{A}) = -0.000776 + 0.0328C (\mu\text{M})$, with the correlation coefficient $R^2 = 0.999$, was obtained in the range of 0.1–27.1 μM , and a different linear correlation equation of $I (\mu\text{A}) = 0.290 + 0.0221C (\mu\text{M})$, with the correlation coefficient $R^2 = 0.999$, was obtained in the range of 27.1–113.4 μM (Figure 4b). The limit of detection (LOD) was calculated to be 0.02 μM , based on the equation $\text{LOD} = 3S_b/k$, where S_b is the average standard deviation of the signals obtained in blank solution and k is the slope of the correlation equation in the low SMZ concentration range. The relative standard deviation (RSD) of 7.9% was obtained by taking 10 continuous measurements of 5.0 μM SMZ in 0.1 M sulfuric solution. This RSD value indicated the good repeatability of the sensor. Another carefully stored $\text{CeVO}_4/\text{MWCNTs-GCE}$ sensor was used to monitor the same concentration of SMZ solution for 7 consecutive days and the RSD was calculated to be 8.4%. Therefore, the stability of the sensor was also satisfactory.

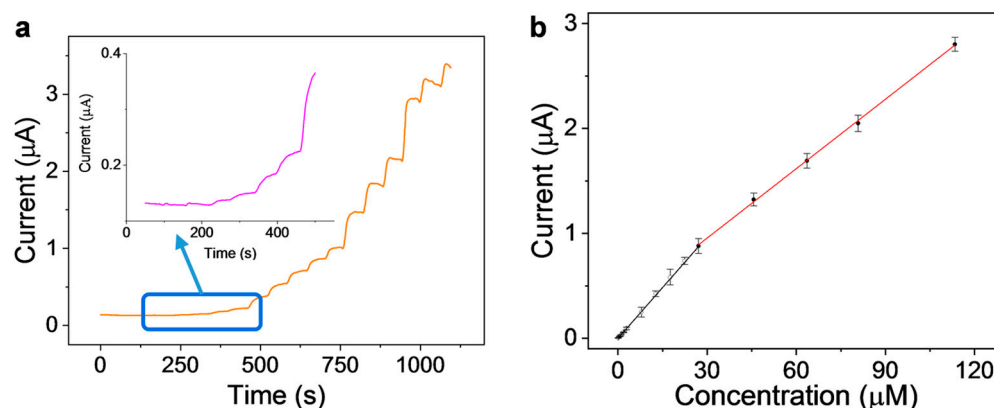


Figure 4. Analytical performance of $\text{CeVO}_4/\text{MWCNTs-GCE}$. (a) Amperometric current-time response curve obtained by the successive addition of different concentrations of SMZ; (b) anodic current versus SMZ concentration plot.

For comparison with literature results, recently published works about sulfonamide testing were listed in Table 1. Although the present work was not the best, the LOD and linear range were better than most of the literature work listed in Table 1. The pH of the supporting electrolyte is a factor that potentially influences the test. As discussed in our previous work [46], with the pH value decreasing, it not only increases the solubility of the sulfonamides, but also promotes the involvement of protons in the electrochemical oxidation of the sulfonamides. Therefore, the whole testing process needed to be controlled in an acidic environment, and 0.1 M dilute sulfuric acid was optimized as the supporting electrolyte. The main interference during sensing was caused by the anodic reaction of substances with oxidation potentials lower than 0.9 V. This would affect the measurement accuracy during the amperometric measurement of SMZ. Therefore, a measurement strategy to carefully eliminate interference was proposed to test real samples. Briefly, the anodic current of a sample (I_0) was recorded under the working potential of 0.9 V, while the background interference current (I_b) was measured at 0.8 V. The real anodic current response (I)

toward SMZ was calculated by subtracting I_b from I_0 . Finally, the exact SMZ content in the samples was calculated according to the regression equation mentioned above. Interference from most potential substances (such as uric acid, ascorbic acid, dopamine, and other inorganic metal ions) was successfully eliminated by this strategy. The potential influence of ionic strength and nature organic matters (NOM) can also be eliminated by this method.

Table 1. Comparison of analytical performance between literature works and this work.

Method	Analyte	LOD (μM)	Linear Range (μM)	Reference
LSV (MIP/Ni(OH) ₂ /NF)	SPy	0.4	0.6–1340	[51]
SWV (SPCE)	SMZ	0.16	1.0–500	[52]
DPV (AuNPs/Gr/GCE)	SAM	0.01	0.1–1000	[53]
DPV (MIP/CNT@COF/GCE)	SMR	0.1	0.3–200	[54]
DPV (GO/ZnO)	SMX	0.029	0.1–1.5	[55]
AuNP/TCBt/GCE	SMZ	0.097	0.89–107.7	[1]
i-t (SmVO ₄ @GOS/GCE)	SSZ	0.002	0.02–667	[56]
i-t (MIP)	SMX		0.8–170	[57]
i-t (CeVO ₄ /MWCNTs-GCE)	SMZ	0.02	0.1–113.4	This work

SPy: sulfapyridine, SSZ: sulfasalazine, SAM: Sulfanilamide, SMR: sulfamerazine, SDM: sulfadimethoxine, SG: sulfaguanidine, LSV: linear sweep voltammetry, SWV: square wave voltammetry, DPV: differential pulse voltammetry.

3.6. Determination of SMZ in Real Samples

The potential of the CeVO₄/MWCNTs-GCE sensor for practical applications was verified by analyzing the trace SMZ residue in aquaculture water samples collected from a fish farm in Qiantang District, Hangzhou, China. First, 5.0 mL samples of the collected water were piped into three clean 10 mL volumetric flasks. Next, 1.0 mL sulfuric acid solution was added to each flask. A different volume of SMZ stock solution was injected into each flask to obtain spiked concentrations of 0, 5.0, and 30.0 μM . Finally, the three flasks were diluted to 10 mL with deionized water, and an amperometric analysis was separately carried out for each flask. As shown in Table 2, no SMZ residue was observed in sample 1, suggesting that the aquaculture water of the fish farm was not polluted by sulfonamides. The recoveries of the two spiked samples were 109% and 93.0%. The RSD values of the two spiked samples were 6.06% and 5.56%, implying that the prepared sensor was sensitive, reliable, and stable.

Table 2. Application of CeVO₄/MWCNTs-GCE toward SMZ detection in real aquaculture water samples.

Sample	Spiked Concentration (μM)	Detected Concentration (μM)	Recovery (%)	RSD (%)
1	0	0	—	—
2	5.0	5.47	109	6.1
3	30.0	27.9	93.0	5.6

4. Conclusions

In summary, a CeVO₄/MWCNTs nanocomposite was prepared by a simple hydrothermal reaction and characterized in detail. The electroanalytical performance of this nanocomposite was assessed by measuring the antibacterial drug SMZ in water samples. Encouragingly, the CeVO₄/MWCNTs nanocomposite exhibited promising catalytic activity for SMZ detection. The CeVO₄/MWCNTs-GCE sensor presented remarkable sensitivity, good selectivity, a lower LOD, and a wide linear response range. Furthermore, the interference of co-existing substances was successfully eliminated by background subtraction. This sensor was also successfully applied to the detection of SMZ in real aquaculture water samples, showing reliable recovery and accuracy. Based on the excellent performance and manu-

facturing convenience of the CeVO₄/MWCNTs-GCE composite, this sensor is expected to be useful for designing and manufacturing online or portable devices for sulfonamide residue measurements.

Author Contributions: X.H. and J.L. contributed to the conception of the study and the supervision of the whole study; J.M. and C.Z. performed the experiments; J.M., X.H. and J.L. significantly contributed to the data analysis, production of drafts, and manuscript preparation. All authors have read and agreed to the published version of the manuscript.

Funding: This research was funded by the Science and Technology Plan Project of Zhejiang Province (Grant No. 2020C03087) and the Zhejiang Provincial Natural Science Foundation of China (LY20B050007).

Institutional Review Board Statement: Not applicable.

Informed Consent Statement: Not applicable.

Data Availability Statement: The data presented in this study are available on request from the corresponding author.

Conflicts of Interest: The authors declare no conflict of interest.

References

1. Lalmalsawmi, J.; Tiwari, D.; Lee, S.M.; Kim, D.J.; Kim, H. Efficient electrochemical sensor for trace detection of sulfamethazine in spring water: Use of novel nanocomposite material coated with Ag or Au nanoparticles. *Microchem. J.* **2022**, *179*, 107520. [[CrossRef](#)]
2. Zhao, H.; Cao, Z.; Liu, X.; Zhan, Y.; Zhang, J.; Xiao, X.; Yang, Y.; Zhou, J.; Xu, J. Seasonal variation, flux estimation, and source analysis of dissolved emerging organic contaminants in the Yangtze Estuary, China. *Mar. Pollut. Bull.* **2019**, *1215*, 208–215. [[CrossRef](#)] [[PubMed](#)]
3. Patyra, E.; Przeniosła-Siwczyńska, M.; Kwiatek, K. Determination of sulfonamides in feeds by high-performance liquid chromatography after fluorescamine precolumn derivatization. *Molecules* **2019**, *24*, 452. [[CrossRef](#)] [[PubMed](#)]
4. Jansomboon, W.; Boontanon, S.K.; Boontanon, N.; Polprasert, C.; Chau, T.D. Monitoring and determination of sulfonamide antibiotics (sulfamethoxydiazine, sulfamethazine, sulfamethoxazole and sulfadiazine) in imported Pangasius catfish products in Thailand using liquid chromatography coupled with tandem mass spectrometry. *Food Chem.* **2016**, *212*, 635–640. [[CrossRef](#)]
5. Zhang, Z.; Liu, J.F.; Shao, B.; Jiang, G.B. Time-resolved fluoroimmunoassay as an advantageous approach for highly efficient determination of sulfonamides in environmental waters. *Environ. Sci. Technol.* **2010**, *44*, 1030–1035. [[CrossRef](#)] [[PubMed](#)]
6. Shelver, W.L.; Shappell, N.W.; Franek, M.; Rubio, F.R. ELISA for sulfonamides and its application for screening in water contamination. *J. Agric. Food Chem.* **2008**, *56*, 6609–6615. [[CrossRef](#)]
7. Wei, X.; Luo, X.; Xu, S.; Xi, F.; Zhao, T. A flexible electrochemiluminescence sensor equipped with vertically ordered mesoporous silica nanochannel film for sensitive detection of clindamycin. *Front. Chem.* **2022**, *10*, 872582. [[CrossRef](#)]
8. Zhang, M.; Zou, Y.; Zhou, X.; Yan, F.; Ding, Z. Vertically-ordered mesoporous silica films for electrochemical detection of Hg(II) ion in pharmaceuticals and soil samples. *Front. Chem.* **2022**, *10*, 952936. [[CrossRef](#)]
9. Lv, N.; Qiu, X.; Han, Q.; Xi, F.; Wang, Y.; Chen, J. Anti-Biofouling electrochemical sensor based on the binary nanocomposite of silica nanochannel array and graphene for doxorubicin detection in human serum and urine samples. *Molecules* **2022**, *27*, 8640. [[CrossRef](#)]
10. Zou, Y.; Zhou, X.; Xie, L.; Tang, H.; Yan, F. Vertically-ordered mesoporous silica films grown on boron nitride-graphene composite modified electrodes for rapid and sensitive detection of carbendazim in real samples. *Front. Chem.* **2022**, *10*, 939510. [[CrossRef](#)]
11. Zheng, W.; Su, R.; Yu, G.; Liu, L.; Yan, F. Highly sensitive electrochemical detection of paraquat in environmental water samples using a vertically ordered mesoporous silica film and a nanocarbon composite. *Nanomaterials* **2022**, *12*, 3632. [[CrossRef](#)] [[PubMed](#)]
12. Gong, J.; Zhang, T.; Chen, P.; Yan, F.; Liu, J. Bipolar silica nanochannel array for dual-mode electrochemiluminescence and electrochemical immunosensing platform. *Sens. Actuat. B Chem.* **2022**, *368*, 132086. [[CrossRef](#)]
13. Yang, L.; Zhang, T.; Zhou, H.; Yan, F.; Liu, Y. Silica nanochannels boosting Ru(bpy)₃²⁺-mediated electrochemical sensor for the detection of guanine in beer and pharmaceutical samples. *Front. Nutr.* **2022**, *9*, 987442. [[CrossRef](#)] [[PubMed](#)]
14. Chen, H.; Huang, J.; Zhang, R.; Yan, F. Dual-mode electrochemiluminescence and electrochemical sensor for alpha-fetoprotein detection in human serum based on vertically ordered mesoporous silica films. *Front. Chem.* **2022**, *10*, 1023998. [[CrossRef](#)]
15. Zhou, H.; Ding, Y.; Su, R.; Lu, D.; Tang, H.; Xi, F. Silica nanochannel array film supported by β-cyclodextrin-functionalized graphene modified gold film electrode for sensitive and direct electroanalysis of acetaminophen. *Front. Chem.* **2022**, *9*, 812086. [[CrossRef](#)] [[PubMed](#)]
16. Liu, Q.; Zhong, H.; Chen, M.; Zhao, C.; Liu, Y.; Xi, F.; Luo, T. Functional nanostructure-loaded three-dimensional graphene foam as a non-enzymatic electrochemical sensor for reagentless glucose detection. *RSC Adv.* **2020**, *10*, 33739–33746. [[CrossRef](#)]

17. Deng, X.; Lin, X.; Zhou, H.; Liu, J.; Tang, H. Equipment of vertically-ordered mesoporous silica film on electrochemically pre-treated three-dimensional graphene electrodes for sensitive detection of methidazine in urine. *Nanomaterials* **2023**, *13*, 239. [[CrossRef](#)]
18. Li, Y.; Gu, X.; Zhao, J.; Xi, F. Fabrication of a ratiometric fluorescence sensor based on carbon dots as both luminophores and nanozymes for the sensitive detection of hydrogen peroxide. *Molecules* **2022**, *27*, 7379. [[CrossRef](#)]
19. Wan, Y.; Zhao, J.; Deng, X.; Chen, J.; Xi, F.; Wang, X. Colorimetric and fluorescent dual-modality sensing platform based on fluorescent nanozyme. *Front. Chem.* **2021**, *9*, 774486. [[CrossRef](#)] [[PubMed](#)]
20. Deng, X.; Zhao, J.; Ding, Y.; Tang, H.; Xi, F. Iron and nitrogen co-doped graphene quantum dots as highly active peroxidases for the sensitive detection of l-cysteine. *New J. Chem.* **2021**, *45*, 19056–19064. [[CrossRef](#)]
21. Cui, Y.; Duan, W.; Jin, Y.; Wo, F.; Xi, F.; Wu, J. Ratiometric fluorescent nanohybrid for noninvasive and visual monitoring of sweat glucose. *ACS Sens.* **2020**, *5*, 2096–2105. [[CrossRef](#)] [[PubMed](#)]
22. Zhao, J.; Zheng, Y.; Pang, Y.; Chen, J.; Zhang, Z.; Xi, F.; Chen, P. Graphene quantum dots as full-color and stimulus responsive fluorescence ink for information encryption. *J. Colloid Interface Sci.* **2020**, *579*, 307–314. [[CrossRef](#)]
23. Zhou, H.; Ma, X.; Sailjoi, A.; Zou, Y.; Lin, X.; Yan, F.; Su, B.; Liu, J. Vertical silica nanochannels supported by nanocarbon composite for simultaneous detection of serotonin and melatonin in biological fluids. *Sens. Actuators B Chem.* **2022**, *353*, 131101. [[CrossRef](#)]
24. Chang, Q.; Huang, J.; He, L.; Xi, F. Simple immunosensor for ultrasensitive electrochemical determination of biomarker of the bone metabolism in human serum. *Front. Chem.* **2022**, *10*, 940795. [[CrossRef](#)]
25. Cui, Y.; Duan, W.; Jin, Y.; Wo, F.; Xi, F.; Wu, J. Graphene quantum dot-decorated luminescent porous silicon dressing for theranostics of diabetic wounds. *Acta Biomater.* **2021**, *131*, 544–554. [[CrossRef](#)]
26. Liu, X.; Chen, Z.; Wang, T.; Jiang, X.; Qu, X.; Duan, W.; Xi, F.; He, Z.; Wu, J. Tissue imprinting on 2D nanoflakes-capped silicon nanowires for lipidomic mass spectrometry imaging and cancer diagnosis. *ACS Nano* **2022**, *16*, 6916–6928. [[CrossRef](#)]
27. Kachooangi, R.T.; Musameh, M.M.; Abu-Yousef, I.; Yousef, J.M.; Kanan, S.M.; Xiao, L.; Davies, S.G.; Russell, A.; Compton, R.G. Carbon nanotube-ionic liquid composite sensors and biosensors. *Anal. Chem.* **2009**, *81*, 435–442. [[CrossRef](#)]
28. Kokulnathan, T.; Karthik, R.; Chen, S.M.; Kumar, J.V.; Sakthinathan, S. A cerium vanadate interconnected with a carbon nanofiber heterostructure for electrochemical determination of the prostate cancer drug nilutamide. *Microchim. Acta* **2019**, *186*, 579. [[CrossRef](#)] [[PubMed](#)]
29. Đurović, A.; Stojanović, Z.; Bytešniková, Z.; Kravić, S.; Švec, P.; Přibyl, J.; Richtera, L. Reduced graphene oxide/ZnO nanocomposite modified electrode for the detection of tetracycline. *J. Mater. Sci.* **2022**, *57*, 5533–5551. [[CrossRef](#)]
30. Baby, J.N.; Sriram, B.; Wang, S.F.; George, M. Integration of samarium vanadate/carbon nanofiber through synergy: An electrochemical tool for sulfadiazine analysis. *J. Hazard. Mater.* **2021**, *408*, 124940. [[CrossRef](#)]
31. Kanna Sharma, T.S.; Hwa, K.Y.; Santhan, A.; Ganguly, A. Synthesis of novel three-dimensional flower-like cerium vanadate anchored on graphitic carbon nitride as an efficient electrocatalyst for real-time monitoring of mesalazine in biological and water samples. *Sens. Actuators B Chem.* **2021**, *331*, 129413. [[CrossRef](#)]
32. Shao, Y.; El-Kady, M.F.; Sun, J.; Li, Y.; Zhang, Q.; Zhu, M.; Wang, H.; Dunn, B.; Kaner, R.B. Design and mechanisms of asymmetric supercapacitors. *Chem. Rev.* **2018**, *118*, 9233–9280. [[CrossRef](#)] [[PubMed](#)]
33. Wang, W.L.; Jang, J.; Nguyen, V.H.; Auxilia, F.M.; Song, H.; Jang, K.; Jin, E.M.; Lee, G.Y.; Gu, H.B.; Ham, M.H. Cerium vanadate and reduced graphene oxide composites for lithium-ion batteries. *J. Alloys Compd.* **2017**, *724*, 1075–1082. [[CrossRef](#)]
34. Bokobza, L.; Zhang, J. Raman spectroscopic characterization of multiwall carbon nanotubes and of composites. *Express Polym. Lett.* **2012**, *6*, 601–608. [[CrossRef](#)]
35. Gupta, R.; Singh, B. Chemical modification of carboxylated MWCNTs for enhanced electrical conducting and magnetic properties. *Mater. Sci. Eng. B-Adv.* **2020**, *262*, 114730. [[CrossRef](#)]
36. Bai, L.; Xu, Y.; Liu, A.; Dong, L.; Zhang, K.; Li, W.S.; Zhao, F.G. Unusual graphite fluoride hydrolysis toward unconventional graphene oxide for high-performance supercapacitors and Li-ion batteries. *Chem. Eng. J.* **2022**, *434*, 134639. [[CrossRef](#)]
37. Ponnaiah, S.K.; Prakash, P. A new high-performance supercapacitor electrode of strategically integrated cerium vanadium oxide and polypyrrole nanocomposite. *Int. J. Hydrog. Energy* **2021**, *46*, 19323–19337. [[CrossRef](#)]
38. Xu, M.; Huang, Q.; Chen, Q.; Guo, P.; Sun, Z. Synthesis and characterization of octadecylamine grafted multi-walled carbon nanotubes. *Chem. Phys. Lett.* **2003**, *375*, 598–604. [[CrossRef](#)]
39. Varga, M.; Izak, T.; Vretenar, V.; Kozak, H.; Holovsky, J.; Artemenko, A.; Hulman, M.; Skakalova, V.; Lee, D.S.; Kromka, A. Diamond/carbon nanotube composites: Raman, FTIR and XPS spectroscopic studies. *Carbon* **2017**, *111*, 54–61. [[CrossRef](#)]
40. Yang, H.; Zha, J.; Zhang, P.; Qin, Y.; Chen, T.; Ye, F. Fabrication of CeVO₄ as nanozyme for facile colorimetric discrimination of hydroquinone from resorcinol and catechol. *Sens. Actuators B Chem.* **2017**, *247*, 469–478. [[CrossRef](#)]
41. Yan, L.; Xu, S.; Xi, F. Disposal immunosensor for sensitive electrochemical detection of prostate-specific antigen based on amino-rich nanochannels array-modified patterned indium tin oxide electrode. *Nanomaterials* **2022**, *12*, 3810. [[CrossRef](#)] [[PubMed](#)]
42. Gong, J.; Zhang, T.; Luo, T.; Luo, X.; Yan, F.; Tang, W.; Liu, J. Bipolar silica nanochannel array confined electrochemiluminescence for ultrasensitive detection of SARS-CoV-2 antibody. *Biosens. Bioelectron.* **2022**, *215*, 114563. [[CrossRef](#)] [[PubMed](#)]
43. Mei, B.A.; Lau, J.; Lin, T.; Tolbert, S.H.; Dunn, B.S.; Pilon, L. Physical interpretations of electrochemical impedance spectroscopy of redox active electrodes for electrical energy storage. *J. Phys. Chem. C* **2018**, *122*, 24499–24511. [[CrossRef](#)]
44. Xiao, Y.; Han, G.; Zhou, H.; Li, Y.; Lin, J.Y. Nickel sulfide counter electrodes enhanced by hydrosulphuric acid hydrothermal treatments for use in Pt-free dye-sensitized solar cells. *Electrochim. Acta* **2015**, *155*, 103–109. [[CrossRef](#)]

45. Canales, C.; Ramos, D.; Fierro, A.; Antilén, M. Electrochemical, theoretical and analytical studies of the electro-oxidation of sulfamerazine and norfloxacin on a glassy carbon electrode. *Electrochim. Acta* **2019**, *318*, 847–856. [[CrossRef](#)]
46. Ma, J.; Hong, X. Simple fabrication of reduced graphene oxide—Ionic liquid composite modified electrode for sensitive detection of sulfadiazine. *Int. J. Electrochem. Sci.* **2020**, *15*, 3729–3739. [[CrossRef](#)]
47. Zhao, H.; Liu, X.; Cao, Z.; Zhan, Y.; Shi, X.; Yang, Y.; Zhou, J.; Xu, J. Adsorption behavior and mechanism of chloramphenicols, sulfonamides, and non-antibiotic pharmaceuticals on multi-walled carbon nanotubes. *J. Hazard. Mater.* **2016**, *310*, 235–245. [[CrossRef](#)]
48. Gong, J.; Tang, H.; Wang, M.; Lin, X.; Wang, K.; Liu, J. Novel three-dimensional graphene nanomesh prepared by facile electro-etching for improved electroanalytical performance for small biomolecules. *Mater. Design* **2022**, *215*, 110506. [[CrossRef](#)]
49. Zhu, X.; Xuan, L.; Gong, J.; Liu, J.; Wang, X.; Xi, F.; Chen, J. Three-dimensional macroscopic graphene supported vertically-ordered mesoporous silica-nanochannel film for direct and ultrasensitive detection of uric acid in serum. *Talanta* **2022**, *238*, 123027. [[CrossRef](#)]
50. Su, R.; Tang, H.; Xi, F. Sensitive electrochemical detection of p-nitrophenol by pre-activated glassy carbon electrode integrated with silica nanochannel array film. *Front. Chem.* **2022**, *10*, 954748. [[CrossRef](#)]
51. Liu, Z.; Zhang, Y.; Feng, J.; Han, Q.; Wei, Q. Ni(OH)₂ nanoarrays based molecularly imprinted polymer electrochemical sensor for sensitive detection of sulfapyridine. *Sens. Actuators B Chem.* **2019**, *287*, 551–556. [[CrossRef](#)]
52. Su, Y.L.; Cheng, S.H. A novel electroanalytical assay for sulfamethazine determination in food samples based on conducting polymer nanocomposite-modified electrodes. *Talanta* **2018**, *180*, 81–89. [[CrossRef](#)] [[PubMed](#)]
53. He, B.S.; Yan, X.H. Modifications of Au nanoparticle-functionalized graphene for sensitive detection of sulfanilamide. *Sensors* **2018**, *18*, 846. [[CrossRef](#)] [[PubMed](#)]
54. Sun, Y.; Xu, L.; Waterhouse, G.I.N.; Wang, M.; Qiao, X.; Xu, Z. Novel three-dimensional electrochemical sensor with dual signal amplification based on MoS₂ nanosheets and high-conductive NH₂-MWCNT@COF for sulfamerazine determination. *Sens. Actuators B Chem.* **2019**, *281*, 107–114. [[CrossRef](#)]
55. Senthil Kumar, P.; Sreeja, B.S.; Krishna Kumar, K.; Padmalaya, G. Static and dynamic analysis of sulfamethoxazole using GO/ZnO modified glassy carbon electrode by differential pulse voltammetry and amperometry techniques. *Chemosphere* **2022**, *302*, 134926. [[CrossRef](#)]
56. Rajaji, U.; Raghu, M.S.; Yogesh Kumar, K.; Al-Kahtani, A.A.; Chen, C.P.; Juang, R.S.; Liu, T.Y. Electrocatalytic oxidation and amperometric determination of sulfasalazine using bimetal oxide nanoparticles-decorated graphene oxide composite modified glassy carbon electrode at neutral pH. *Microchim. Acta* **2022**, *189*, 409. [[CrossRef](#)]
57. Turco, A.; Corvaglia, S.; Mazzotta, E.; Pompa, P.P.; Malitesta, C. Preparation and characterization of molecularly imprinted mussel inspired film as antifouling and selective layer for electrochemical detection of sulfamethoxazole. *Sens. Actuators B Chem.* **2018**, *255*, 3374–3383. [[CrossRef](#)]

Disclaimer/Publisher's Note: The statements, opinions and data contained in all publications are solely those of the individual author(s) and contributor(s) and not of MDPI and/or the editor(s). MDPI and/or the editor(s) disclaim responsibility for any injury to people or property resulting from any ideas, methods, instructions or products referred to in the content.